

# Characterization of the crack initiation and propagation in Alloy 600 with a cold-worked surface

Zhao Shen<sup>a,\*</sup>, Kai Chen<sup>b</sup>, David Tweddle<sup>a</sup>, Guanze He<sup>a</sup>, Koji Arioka<sup>c</sup>, Sergio Lozano-Perez<sup>a</sup>

<sup>a</sup> Department of Materials, University of Oxford, Parks Road, OX1 3PH Oxford, UK

<sup>b</sup> School of Nuclear Science and Engineering, Shanghai Jiao Tong University, 800 Dongchuan Road, Shanghai 200240, China

<sup>c</sup> Institute of Nuclear Safety Systems, Inc. (INSS), 64 Sata, Mihama-cho, Mikata-gun, Fuki, Mihama 919-1205, Japan

Corresponding author

Zhao Shen      zhao.shen@materials.ox.ac.uk

## Abstract

The crack initiation on a cold-worked surface of Alloy 600, exposed to simulated pressurized water reactor primary water, was mechanistically studied through high-resolution characterization. Mechanical polishing introduced a thin recrystallization layer on the specimen surface, which lead to the crack initiation along highly-deformed recrystallization grain boundaries after preferential oxidation. Intergranular crack propagation occurred once the initiation cracks met the matrix grain boundaries under the external loading and the residual stress introduced by the prior 20% cold working. The controlling mechanism of SCC crack propagation was believed to be an intergranular selective oxidation mechanism.

**Key words:** Alloy 600; crack initiation; crack propagation; selective oxidation; grain boundary migration.

## 1. Introduction

Stress corrosion cracking (SCC) has been frequently reported in Alloy 600 after exposure to the primary water conditions of pressurized water reactors (PWRs) [1-6]. Since SCC is a synergic effect of material, mechanics, and environment, developing a complete understanding of this behavior is very difficult [1, 2]. Although the tests on SCC propagation of Alloy 600 have been widely conducted and various parameters affecting SCC crack growth have been revealed [1, 7], SCC initiation is less explored due to difficulties in achieving the necessary experimental scale of analysis (micro-to-nano). However, this phenomenon is equally important when accurately predicting the in-service lifetime of this material under specific environments [8, 9].

According to the work conducted in the literature [8-11], surface oxidation properties can significantly affect the process of SCC initiation. Different surface states caused by various sample grinding and polishing could lead to different surface oxidation behaviors [8-11]. In nuclear power plants, the surfaces of field components are rarely well-polished, and are usually coarsely ground, resulting in a superficial cold-worked layer which may influence the crack initiation behavior. Consequently, the role of the surface states in SCC initiation should be carefully clarified. To date, a great deal of work has been conducted in this field, but mainly based on the measurement of different crack initiation times or crack densities caused by different surface states and the conclusions are not consistent [8, 10-12]. To mechanistically understand the effect of surface state on crack initiation, high-resolution characterization has become ever more important [9, 13].

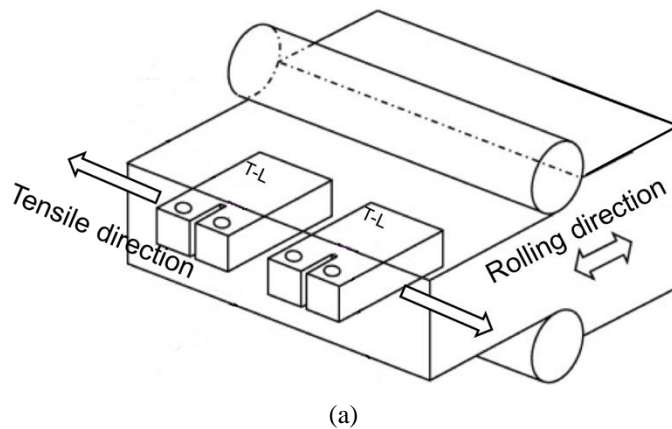
Once a crack initiates from a material surface, crack propagation can occur under the external loading. To date, a number of mechanisms have been proposed to explain the SCC behaviors, including the film rupture mechanism, the hydrogen embrittlement mechanism, the cavity formation mechanism, and the intergranular selective oxidation mechanism [14-22]. Among them, the intergranular selective oxidation mechanism, which

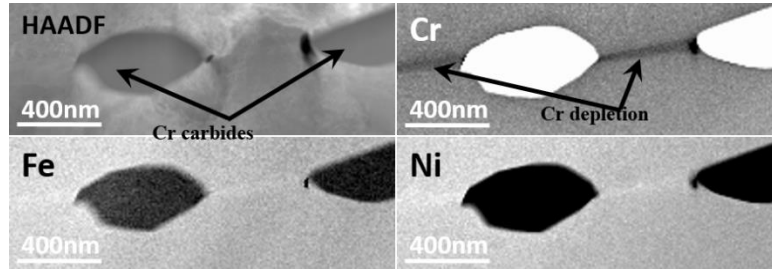
was first proposed by Scott et al. [23] and further developed in the following papers [6, 13, 21, 24, 25], seems to most closely explain the cracking of Alloy 600 in the PWR primary water conditions. According to the intergranular selective oxidation mechanism, the basic assumption is that grain boundaries are preferentially oxidized once exposed to PWR primary water, becoming brittle and, therefore, susceptible to cracking. The brittle mechanical properties of the oxidized grain boundaries under the external loading have been experimentally observed by many researchers [26-28] through micromechanical testing. Although the chemistry and structure of the intergranular oxide ahead of SCC crack tips have been studied by, e.g., Bruemmer et al. [5] and Shen et al. [3] through transmission electron microscopy (TEM), the details of the intergranular selective oxidation in the grain boundaries ahead of SCC crack tips are still unclear, which may help understanding the SCC mechanisms.

In this work, SCC crack initiation and propagation were observed in Alloy 600 with a cold-worked surface, after exposure to simulated PWR primary water. To understand the effects of cold-worked surface on the SCC crack initiation and propagation, high-resolution characterization techniques such as analytical TEM (ATEM) and transmission Kikuchi diffraction (TKD) were used to reveal the underlying mechanisms.

## 2. Material and methods

The Alloy 600 studied in this work was cold-worked and tested under simulated PWR primary water conditions (hydrogenated water: 500 ppm B + 2 ppm Li + 30 ml H<sub>2</sub>/kg water) at 360°C for 355.2h. Cold work in the specimen was produced through uni-directional rolling on a plate at room temperature to a thickness reduction of 20%, which was referred to as 20% cold work. Fig. 1a shows how the 1/2T compact tension (CT) specimen was extracted in T-L direction, which means the crack growth direction was parallel to the rolling direction. It was mill-annealed in air at 930°C followed by water quenching, causing intergranular carbide precipitation. The intergranular carbide coverage was up to 30%. The intergranular carbides were mostly Cr<sub>7</sub>C<sub>3</sub> [3] and the grain boundaries were found depleted in Cr (~12 at.% at grain boundaries vs. ~18 at.% in metal matrix), as shown in Fig. 1b. The SCC testing was conducted using a pre-cracked 0.5T CT specimen with 12.5 mm thickness in an autoclave under a constant load of 30 MPa·m<sup>1/2</sup> [1]. The CT specimen was manufactured by electric discharge machining (EDM). To remove the EDM-affected zone, the surfaces of the CT specimen were ground using SiC papers up to 800 grit. The material composition is shown in Table 1. Before destructive examination of the fracture surface, one piece of cross-section sample (containing an out surface) was cut out from the CT specimen after the autoclave testing for the following analysis.





(b)

Fig. 1. (a) Illustration of 20% cold-worked 1/2T CT specimen tested in T-L orientation; (b) HAADF image and EELS chemical composition maps showing intergranular Cr-depletion.

Table 1 Chemical composition of the alloy used in this study (wt%).

Material	C	Cr	Fe	Si	Mn	P	S	Cu	Ni
Alloy 600	0.06	16.02	6.94	0.33	0.35	0.006	<0.001	0.03	76.26

A dual beam Zeiss NVision 40 focused ion beam (FIB) was used to prepare TEM foils containing SCC cracks. Once the TEM samples were prepared, high-resolution scanning TEM (STEM) and electron energy loss spectroscopy (EELS) were conducted with a JEOL ARM200F (cold-field emission gun) operating at 200 kV and equipped with a Quantum Gatan image filter (GIF). To understand the metallographic information under the grinding surface and around the crack tips, TKD was performed using a Zeiss Crossbeam 540 FEG-SEM equipped with an Oxford Instrument (OI) electron backscattered diffraction (EBSD) Nordlys Max 3 detector. Image quality, misorientation (MO), kernel MO (KMO), and inverse pole figure (z-axis) (IPFZ) maps were calculated automatically by OI software Channel 5, and MO line profiles extracted manually to calculate the dislocation density around the crack tips. The step size was set to 10 nm.

### 3. Results

#### 3.1 Morphology and metallography of the cold-worked surface

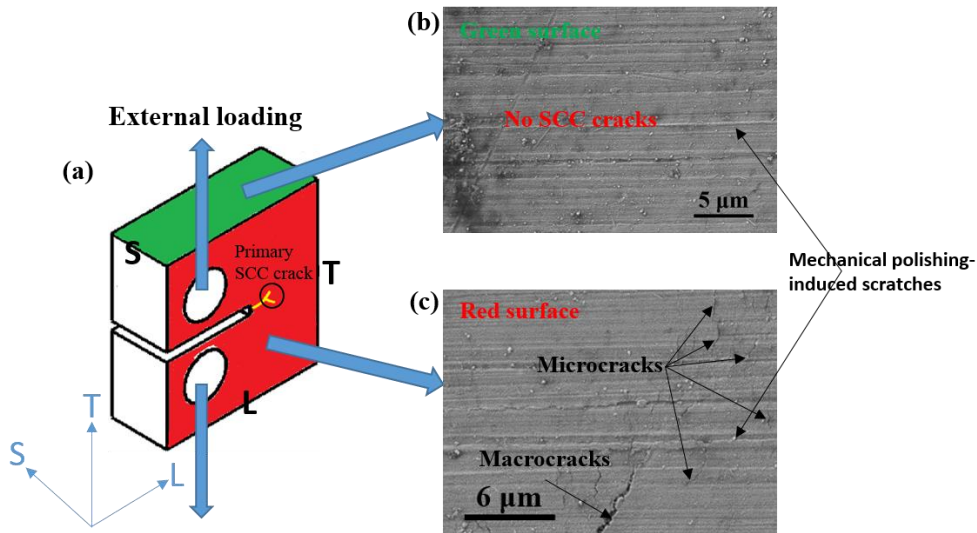


Fig. 2. (a) A schematic of 0.5T CT specimen; (b) SEM image showing a crack-free surface; (c) SEM image showing the existence of microcracks and macrocracks.

SEM imaging was conducted on the outer surfaces of the CT specimen after the autoclave testing. As shown

in Fig. 2a, during the SCC testing, the external loading mainly concentrated at the primary SCC crack tips. Compared with the red surface, the external loading did not affect the green surface. After the SCC testing, no SCC cracks were observed on the green surface under the SEM examination, as shown in Fig. 2b. However, many macrocracks and microcracks can be observed on the red surface and nearly all cracks were oriented perpendicular to the direction of the external loading, as shown in Fig. 2c. The distance between the examined region shown in Fig. 2c and the primary SCC crack was around 10 mm. Since the surfaces were not polished to a smooth finish, many scratches were observed (see Figs. 2b and c).

A cold-worked surface has been reported to have significant effect on SCC initiation [8-10, 13]. To understand the underlying connections between the cold-worked surface and the crack initiation, several TEM samples containing the cross-section of SCC cracks (macrocracks and microcracks) were prepared from the red surface and then analyzed. TKD was firstly conducted on the TEM samples taken from the mechanically-polished surface prior to the SCC test. A typical result is shown in Fig. 3, where a deformation layer consisting of recrystallized grains is clearly observed (see Figs. 3a and b). The thickness of the deformation layer was not uniform, ranging from 200 to 700 nm. The KMO map in Fig. 2c shows a large concentration of dislocations in the deformation layer, especially at the grain boundaries of these recrystallized grains. The unindexed region was marked as black in the TKD maps.

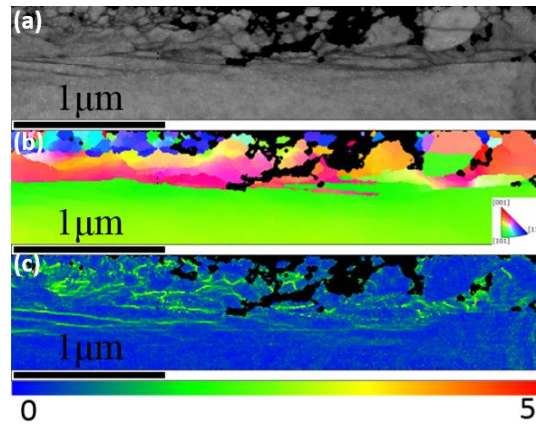


Fig. 3. Typical cross-sectional TKD analysis acquired at the region close to the grinding surface (step size = 10 nm): (a) image quality map; (b) IPFZ map (along normal axis); (c) KMO map.

### 3.2 ATEM characterization of the deformation layer

#### 3.2.1 Characterization of the macrocracks

Three TEM foils containing macrocracks were extracted from the red surface (see Fig. 2a). The position of one of the TEM foils containing a macrocrack is shown in Fig. 4a, which is around 10 mm away from the primary SCC crack. According to the work conducted by Xue et al. [14], the calculated stress around this region was ~400 MPa. The typical feature of the macrocrack is schematically shown in Fig. 4b. The TEM sample preparation process is shown in Fig. 4c. The depth of this macrocrack was around 8  $\mu\text{m}$  and the average depth of the three examined macrocracks was around 10  $\mu\text{m}$ . All the macrocracks examined in this study were observed to be intergranular. To understand how the macrocrack initiated along the grain boundary, the deformation layer close to the macrocrack was examined in detail by analytical TEM (ATEM). As shown in Fig. 4b, Region 1 represents the typical features in the region connected to the macrocrack; Region 2 represents the typical features in the region around 2-7  $\mu\text{m}$  away from the macrocrack; and Region 3 represents the typical features around the macrocrack tip.

High angle annular dark field (HAADF) imaging, middle angle annular dark field (MAADF) imaging,

Fresnel contrast TEM imaging, and EELS were conducted on the Region 1 (see Fig. 4b) and the corresponding results are shown in Figs. 5a-d, respectively. Fig. 5a shows that the deformation layer close to the macrocrack has suffered severe oxidation. In addition, a large concentration of micro-pores were observed in the oxide. Further observation reveals a thin layer of oxide film existing on the outer surface, and the structure of this oxide film seemed to be more compact than the oxide under the surface (see Figs. 5a and b). The EELS elemental analysis shows that the chemical composition in the outer surface oxide was 20.2-23.5% Cr, 53.1-56.5% O, 8.5-11.1% Fe, and 9.3-19.5% Ni in atomic percentage, while the chemical composition in the oxide under the surface was 27.6-34.1% Cr, 56.1-56.5% O, 3.4-4.1% Fe, and 4.5-8.5% Ni in atomic percentage. It is interesting to note that Region 1 was not completely oxidized, with the presence of small grains surrounded by oxide. The formation of these small grains was caused by surface grinding prior to the autoclave testing (see Fig. 3). Since MAADF image is very sensitive to the material orientation, the different signal intensities of the small grains and the base metal suggest that they might have different orientations, which was consistent to the TKD analysis. In order to properly reveal the porous structure in Region 4 (see Fig. 5b), Fresnel contrast TEM imaging with defocus value of  $\pm 800$  nm was conducted. No pores were observed in the small grains surrounded by the oxide and also within the base metal (see Fig. 5c), which suggested that the formation of pores in the oxide might be due to oxidation. In addition, the Fresnel contrast TEM images also show that the oxide in the deformation layer was more porous than the outer surface oxide. Fig. 5d illustrates the elemental distribution in Region 5 (see Fig. 5a). The oxide was enriched in Cr and depleted in Ni and Fe. The content of Cr in the oxide was not uniform. Although the morphology of the small grains was similar to the unaffected matrix, the elemental maps reveal that the chemical composition in the small grains has been changed. Compared with the unaffected matrix, the small grains were enriched in Ni while depleted in Cr and Fe.

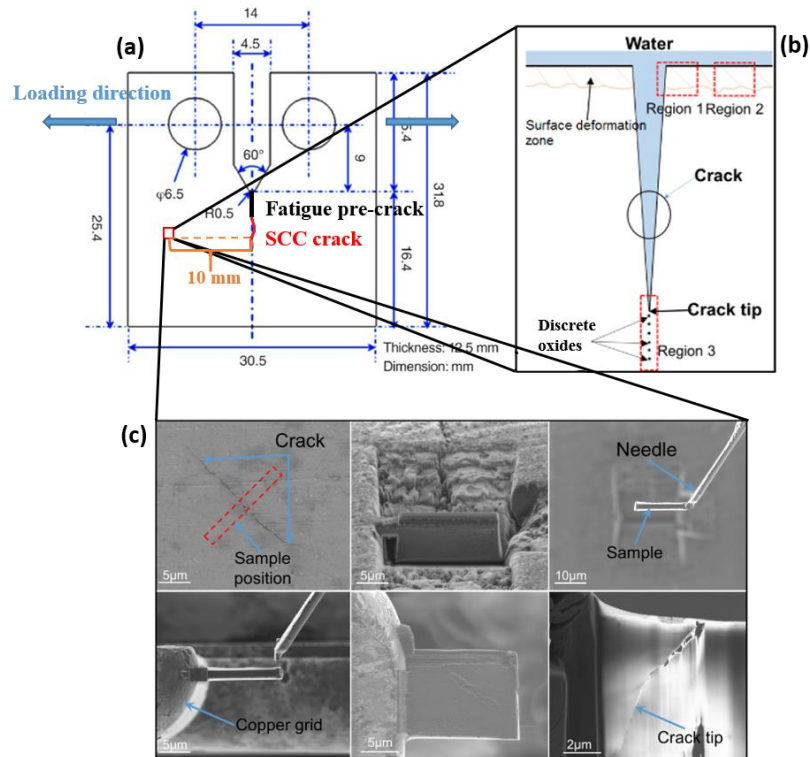


Fig. 4. (a) The dimensions of the 0.5T CT specimen used in this study; (b) schematic illustration of a TEM sample containing the cross-section of an initiation crack; (c) SEM images showing the cross-section TEM sample preparation process.



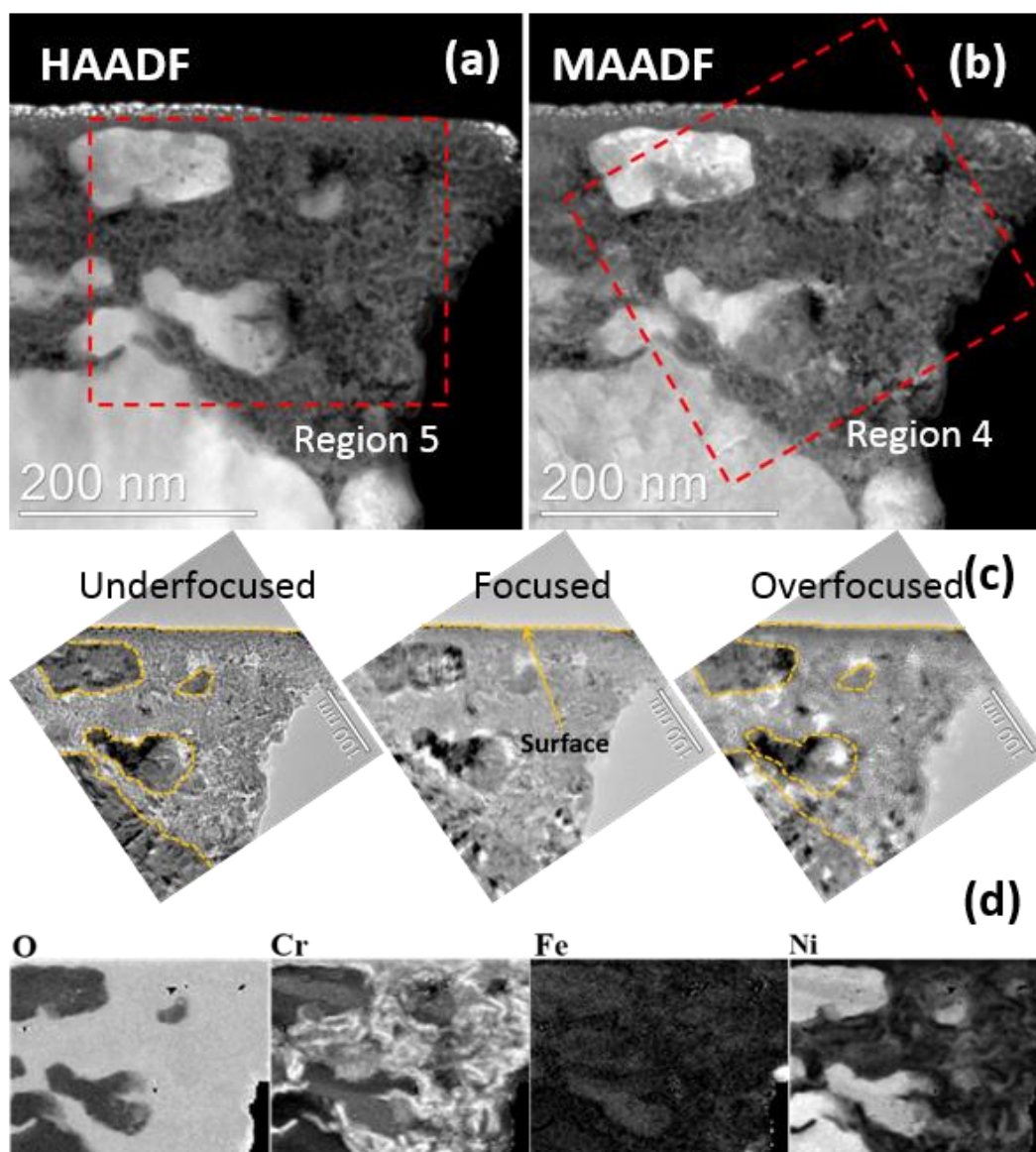


Fig. 5. Structure and chemistry in the Region 1 where is close to a grain boundary after autoclave testing: (a) HAADF image; (b) MAADF image; (c) Fresnel contrast TEM images of the Region 4 in (b) with defocus value of  $\pm 800$  nm; (d) EELS elemental mapping of Region 5 in (a) with a temperature scale bar.

Similar analysis was also conducted on Region 2 (see Fig. 4b), which is approximately  $3\ \mu\text{m}$  away from the macrocrack. A deformation layer consisting of small grains was clearly observed below a uniform surface oxide film, as shown in Figs. 6a and b. Oxidation was also observed to develop into the deformation layer along the newly formed grain boundaries with much greater porosity than the outer surface oxide. Although the outer surface oxide appeared to be able to inhibit the intragranular oxidation, the intergranular oxidation was not effectively prevented. The chemical composition in the surface oxide and the intergranular oxide was similar to those observed in Region 1 (see Fig. 5d), enriched in Cr, while the Fe and Ni were found to be depleted, as shown in Fig. 6d. The Fresnel contrast TEM images further evidence that the structure of the surface oxide has lower porosity than the intergranular oxide (see Fig. 6c). Compared with Region 2, the oxidation in Region 1 was more severe, which might be because it was closer to the macrocrack, enabling a substantial exposure to the PWR water.

The oxide in the deformation layer was mainly composed of Cr and O (see Fig. 6), indicating that Cr was selectively oxidized. Although the selective oxidation of less-noble solute elements in the materials is generally

known as internal oxidation, it was not until 1959 that it was thoroughly analyzed and formalized by Wagner [29]. Internal oxidation is used in the generic sense in which a diffusing species from the surface reacts with a less-noble solute in the alloy to form internal oxides. In the current study, the less-solute element is Cr. In the study of SCC in Alloy 600, Scott et al. [16] found selective oxidation of Cr at grain boundaries, which was initially defined as intergranular internal oxidation and then an internal oxidation mechanism was proposed as a possible SCC mechanism by the authors. However, according to the classic internal oxidation theory [29], to support the occurrence of internal oxidation, an observation of discrete oxide precipitates is prerequisite. Although the intergranular selective oxidation of Cr has been frequently reported [3, 6, 13, 21, 24, 25, 30], there is still no solid evidence to show the existence of discrete oxide precipitates. As a result, the internal oxidation mechanism was modified to be the intergranular selective oxidation mechanism by the subsequent researchers [6, 13, 21, 24, 25].

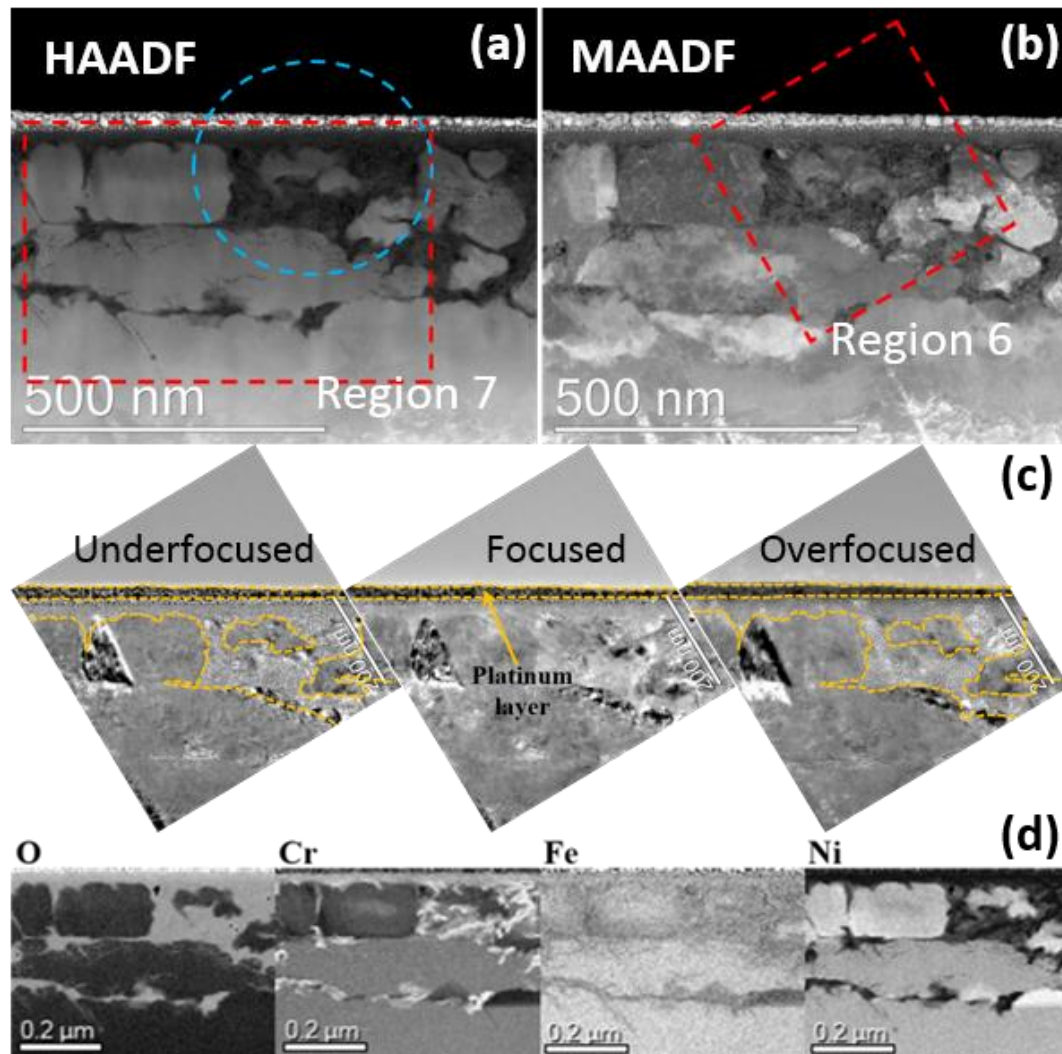


Fig. 6. Structure and chemistry in the Region 2 where is far away from a grain boundary after autoclave testing: (a) HAADF image; (b) MAADF image; (c) Fresnel contrast TEM images of Region 6 in (b) with defocus value of  $\pm 800$  nm; (d) EELS elemental mapping of Region 7 in (a) with a temperature scale bar.

As shown in Fig. 6a, although the oxidation in the deformation layer was mainly along the recrystallized grain boundaries, oxidation was also observed to propagate into the recrystallized grains (marked by a blue dashed circle). To reveal the relationship between the intergranular oxidation and the intragranular oxidation in the deformation layer, higher resolution imaging and EELS mapping were conducted, as shown in Fig. 7. Fig. 7a

shows that the oxidation in the recrystallized grains appeared to initiate from the intergranular oxides. The intragranular oxides (black dots in Fig. 7a) seemed discretely distributed, within the limitations of the 2D elemental maps, which could support the classical internal oxidation model proposed by Wagner [29]. In addition, as mentioned above, the internal oxidation will lead to the selective oxidation of Cr. According to the EELS elemental maps shown in Fig. 7b, the intragranular oxides were enriched in Cr and depleted in Fe and Ni, which also supported the internal oxidation model. However, the results shown in Fig. 7 can only prove that the intragranular oxides were discrete in 2 dimensions (2D) and these oxides might be interconnected in 3 dimensions (3D). To prove these oxides are discrete in 3D, a 3D characterization technique is needed, such as atom probe tomography (APT).

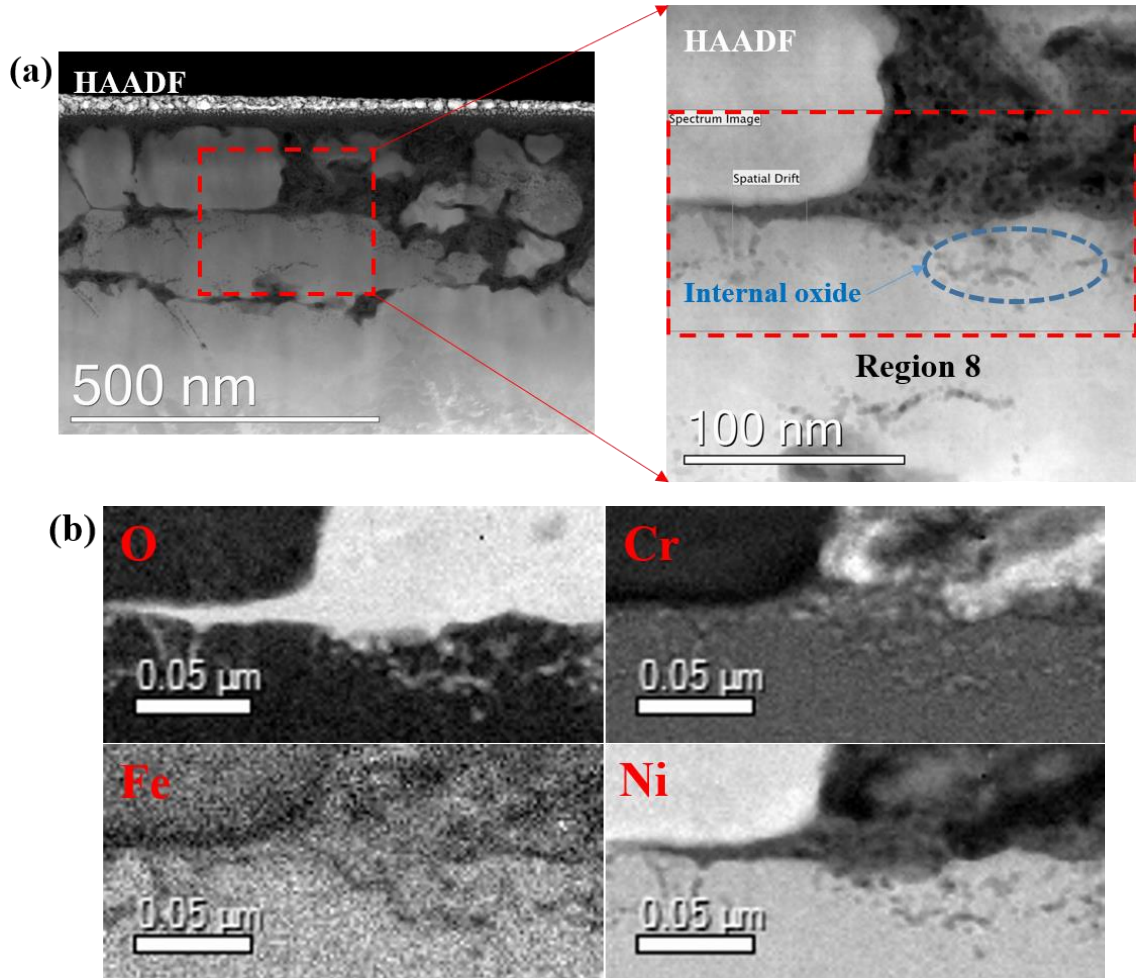


Fig. 7. (a) Magnified HAADF image showing the internal oxidation in a recrystallized grain; (b) EELS elemental maps showing the chemical composition of the internal oxides in a recrystallized grain (Region 8).

### 3.2.2 Characterization of the microcracks

The microcracks initiated on the red surface (see Fig. 2) were also characterized by high-resolution ATEM. Two TEM foils containing many microcracks were prepared and one typical result is shown in Fig. 8. The TEM foil shown in Fig. 8 was prepared from the region close to the macrocrack shown in Fig. 5 and was also around 10 mm away from the primary SCC crack. Both the microcracks and deformation layer can be observed in the HAADF and MAADF images, respectively (see Figs. 8a and b). Further observation reveals that nearly all microcracks propagated along the grain boundaries of the recrystallized grains and terminated at the front of deformation layer (see Fig. 8b). To see the chemical composition around the microcracks, one microcrack marked



by the red dashed rectangle (Region 9 in Fig. 8a) was analyzed by EELS. As shown in Fig. 8c, the oxidation in the deformation layer was mainly intergranular, although intragranular oxidation was also observed, which was similar to what was observed in Fig. 6. In addition, all the oxides were also enriched in Cr and depleted in Fe and Ni, suggesting that Cr was selectively oxidized. Further observation around the crack tip of the microcrack reveals that the microcrack terminated at the front of deformation layer and the oxidation ahead of the microcrack tip was minimum.

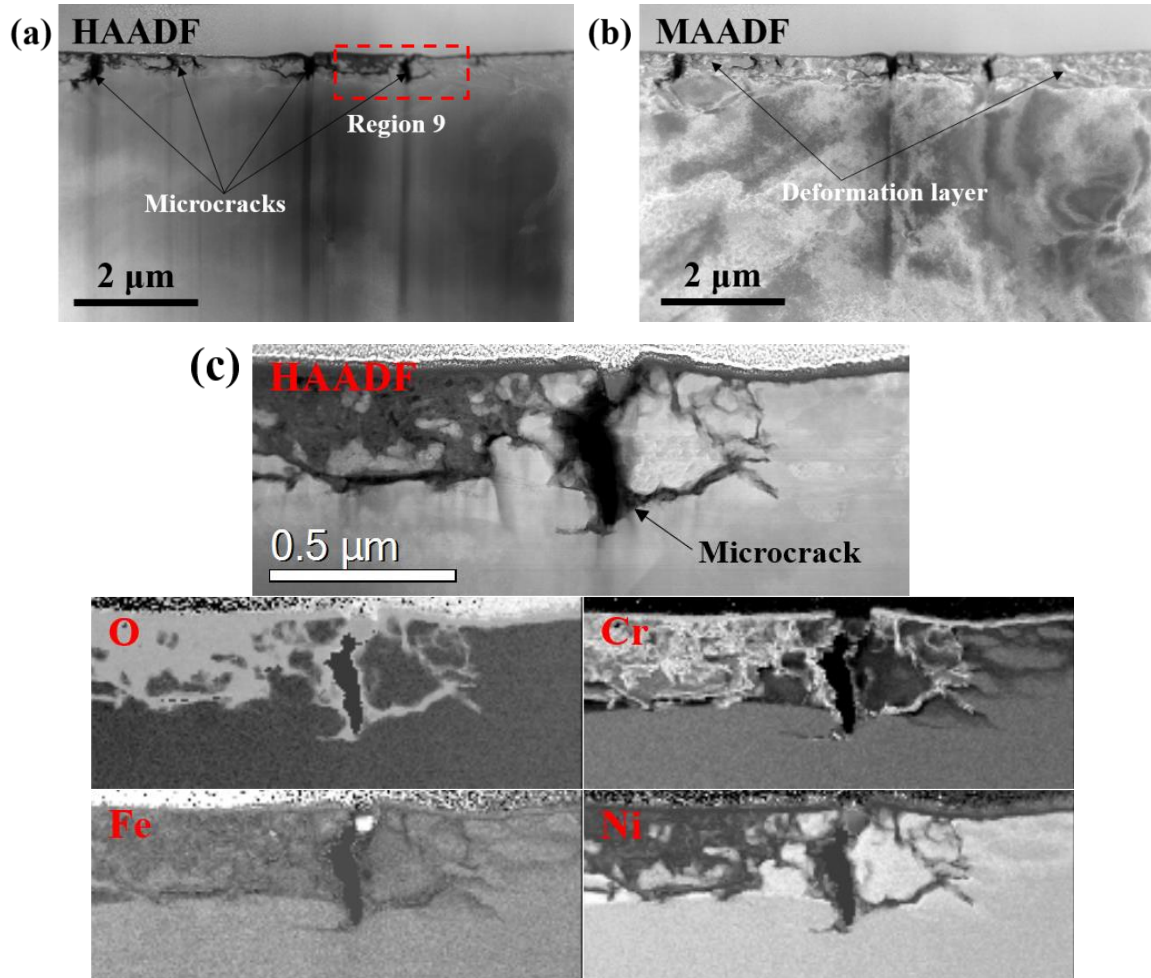


Fig. 8. (a) HAADF and (b) MAADF images showing the microcracks in the deformation layer; (c) HAADF image and related EELS elemental maps of Region 9.

### 3.3 Characterization of the macrocrack tips

As shown in Fig. 2a, many macrocracks were observed on the red surface. The average depth of the macrocracks was around 10 μm, much longer than the microcracks (less than 1 μm). Since all the examined macrocracks were intergranular (along the original matrix grain boundaries), to understand the SCC propagation mechanism, three TEM samples containing SCC macrocracks were prepared and the region around the crack tips were characterized via high-resolution ATEM and TKD.

#### 3.3.1 ATEM characterization

The cross-section morphology of a typical macrocrack tip is shown in Fig. 9a (Region 3 in Fig. 4b). The crack flanks were oxidized after exposure to the high-temperature water. In addition, the oxidation did not stop at the crack tip but propagated into the grain boundary ahead of the crack tip, forming an intergranular oxidation zone (IOZ) with a length of around 350 nm, as shown in Fig. 9b. Further observation reveals that the IOZ was not

continuous and some discretely distributed oxide particles were observed (see the dark spots in Fig. 9a). EELS elemental maps in Fig. 9b show a very long Cr/Fe-depleted while Ni-enriched region ahead of the crack tip. The oxide in IOZ was enriched in Cr and depleted in Fe and Ni. The discretely distributed oxide particles were observed ahead of all examined macrocrack tips and they were all enriched in Cr and depleted in Fe and Ni, which supported the classic internal oxidation model [29], as shown in Fig. 10. Limited by the 2D characterization, the discrete oxide particles observed ahead of the macrocrack tips also might be interconnected in 3D.

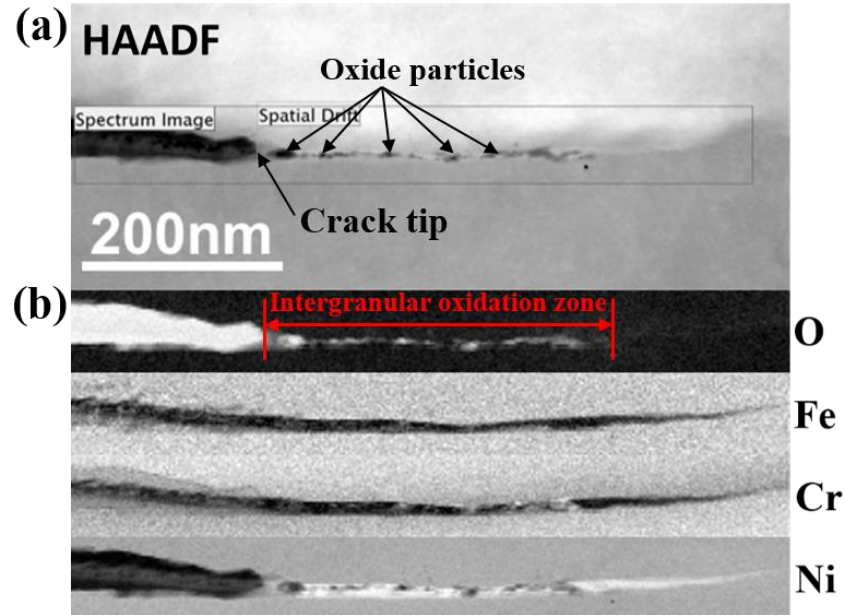


Fig. 9. Structure and chemistry in Region 3 where is around a crack tip after autoclave testing: (a) HAADF image; (b) EELS elemental maps.

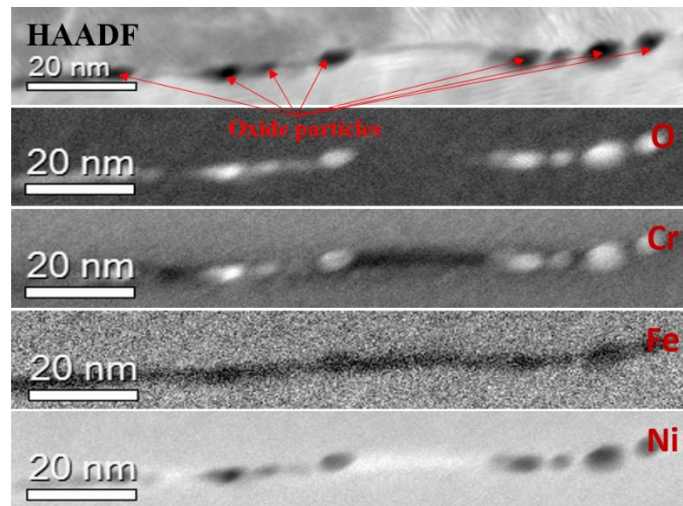


Fig. 10. HAADF image and corresponding EELS elemental maps showing the morphology and chemical composition in the grain boundary ahead of a crack tip.

### 3.3.2 TKD characterization

According to the recent works conducted by Shen et al. [3] and Meisnar et al. [15], the external loading could lead to localized deformation around the SCC crack tips, which could not only introduce a localized deformation zone (LDZ) around the crack tips to enhance intergranular oxidation, but also work as a driving force to break the oxidized grain boundaries and result in crack propagation. To experimentally reveal the existence of the localized

deformation around the SCC crack tips, TKD analysis was conducted. More details regarding this technique can be found in [3, 15].

A typical result is shown in Figs. 11a-c. Two MO line profiles were extracted from the crack tip outwards into the two grains, as shown in Fig. 11d and e. The LDZ sizes in the left and right grains were 215 and 165 nm and the corresponding lattice rotation was  $3.7 \pm 1.1^\circ$  and  $2.7 \pm 1.1^\circ$ . MO line profiles were also extracted from the grain boundary ahead of the crack tip, as shown in the supplementary data (see Fig. S1). The results showed that the lattice rotation in these regions was around 4 times lower than that around the crack tip, indicating that the localized deformation indeed occurred around the crack tip during SCC propagation. It is necessary to point out that the measurement of localized deformation intensities in this study were treated as qualitative.

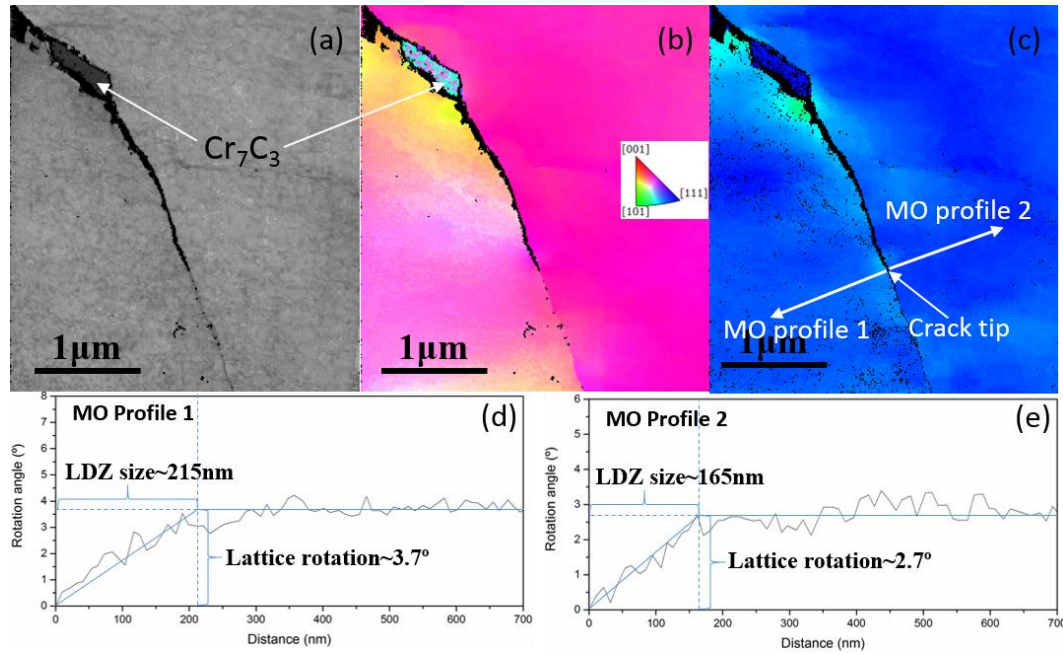


Fig. 11. Typical TKD analysis acquired around the crack tip region (step size = 10 nm): (a) image quality map; (b) IPFZ map (along normal axis); (c) MO map; (d) MO line profile extracted in the left grain; (e) MO line profile extracted in the right grain.

## 4. Discussion

SCC crack initiation and propagation were observed on the cold-worked surface of Alloy 600 after exposure to simulated PWR primary water at 360°C. Utilizing the high-resolution characterization conducted above, the effect of the cold-worked surface on the SCC crack initiation and the mechanism controlling the SCC crack propagation have been studied in detail.

### 4.1 The effect of cold-worked surface on the crack initiation

A thin layer of deformation zone (200-700 nm) consisting of nano-sized recrystallized grains has been revealed by TKD (See Figs. 3a and b). A large number of dislocations introduced by mechanical polishing, were found to exist in this region, especially in the newly formed grain boundaries (see Fig. 3c). Mechanical polishing-induced deformation layer has also been reported by many other researchers [8, 10-13, 31-37]. After exposure to the simulated PWR primary water, a uniform and compact oxide film (less than 50 nm in thickness) formed on the outer surface (see Figs. 4 and 5). The oxidation along the newly formed grain boundaries was not effectively prevented, resulting in intergranular oxidation in the deformation layer. However, the intergranular oxidation in the deformation layer terminated at the deformation layer-metal matrix interface. Defects such as dislocations

were reported to be able to act as short circuits for elemental diffusion, resulting in more severe oxidation [38, 39]. In addition, a high concentration of nano-pores were observed in the intergranular oxide, indicating that the protectiveness of this oxide was poor, which further accelerated the intergranular oxidation. Consequently, it is suggested that the severe intergranular oxidation in the deformation layer was due to the synergistic effects of cold work-induced defects and porous intergranular oxide.

According to the (S)TEM images (see Figs. 5 and 6), the intergranular oxide in the deformation layer was more porous than that next to the outer surface. The EELS analysis revealed that the Cr content in the intergranular oxide was higher than in the outer surface oxide and the contents of Fe and Ni were lower. However, higher content of Cr in the oxide usually entails a more compact structure, which is contradictory to what was observed in this study. In order to address this result, more details regarding the outer surface oxide and the intergranular oxide are required. Since the outer surface oxide was directly exposed to the water, the corrosion potential in this region can be assumed to be higher than in the grain boundaries under the surface oxide film. The higher corrosion potential could oxidize part of the metallic Fe and Ni and form a compact Cr-Fe-Ni spinel. While the lower corrosion potential in the grain boundaries under the surface oxide film could only selectively oxidize Cr, and metallic Fe and Ni were expelled to the surrounding grains adjoining the boundaries and/or solution. According to the work conducted in the literature [3, 5, 11, 16, 23, 40], the selective oxidation of Cr could lead to the separation of Cr oxide precipitates and metallic Fe and Ni, which will inevitably introduce vacancies or pores in the incoherent interfaces of these different phases. Selective oxidation-induced separation of different phases was not only observed by EDX [24] and EELS [3], but also observed via atom probe tomography (APT) [41] and atomic-resolution TEM [42]. Consequently, the nano-pores induced by the selective oxidation might explain why the porosity of the intergranular oxide was higher than the outer surface oxide.

Since oxides are brittle in nature, which has been experimentally proved by many researchers [26-28, 43], SCC cracks will initiate along the oxidized grain boundaries once the external loading is greater than their mechanical strength. Although intergranular oxidation was observed throughout the deformation layer, SCC microcracks were only observed in some regions and some other regions were free of SCC microcracks. This might be because the mechanical polishing led to different extent of deformation in the deformation layer and SCC cracks only initiated in the region with high defect density. This explanation is further supported by the fact that the extent of oxidation in the deformation layer was not uniform, with significant differences between regions (see Figs. 5-8).

According to the work conducted by Arioka et al. [1], SCC cracks were observed to initiate from an oxidized cold-worked surface without external-loading. Similar phenomenon was also reported by other researchers [8, 23]. The authors believed that the superficial compressive stress left after the mechanical polishing could invert locally into highly tensile stresses upon plastic deformation, which could contribute to the external loading to initiate the SCC cracks. As a result, the residual stress left by the mechanical polishing could play a role in accelerating the crack initiation observed in the current study.

It is worth noting that the green surface was subjected to the same mechanical polishing, but no SCC cracks were observed on this surface (see Fig. 2), indicating that the residual stress introduced by the surface grinding alone could not lead to crack initiation. The SCC crack initiation observed on the red surface should be the synergistic effect of the external loading and residual stress. Since no SCC cracks were observed on the green surface, it is logical to rule out the possibility that the cracks observed on the red surface were introduced by the sample preparation and not as a result of SCC initiation.



## 4.2 The mechanism controlling the crack propagation

A large number of SCC cracks were observed on the red surface after the autoclave testing (see Fig. 2). Among them, the majority of cracks terminated at the deformation layer-metal matrix interface. Several cracks were observed to propagate across the deformation layer, propagating deeply into the metal matrix ( $\sim 10\ \mu\text{m}$ ). These cracks always had a larger crack opening than the cracks which terminated at the deformation layer-metal matrix interface. These cracks were termed macrocracks in comparison with the smaller microcracks. Since the propagation of all examined macrocracks were observed to be along the matrix grain boundaries, it is clear that there must be some reasons relating to how initiation cracks become macrocracks when they come into contact with matrix grain boundaries. One possible explanation is that the dislocation density around the matrix grain boundaries was higher than in the grain, which could lead to enhanced oxidation [38, 39]. This hypothesis is possible since the material was 20% cold-worked prior to the autoclave testing. The results from literature [43, 44] show that cold working could lead to the preferential accumulation of dislocations in some grain boundaries with special orientations. Another possible explanation is that the matrix grain boundaries were depleted in Cr due to the carbide precipitation (see Fig. 1b). Once the initiation cracks met the prior Cr-depleted matrix grain boundaries with high content of dislocations, the cracks could further propagate along the grain boundaries under the synergistic effect of intergranular oxidation, external loading, and residual stress.

High-resolution characterization around the crack tips has been proved to be an effective way to obtain a mechanistic understanding of SCC propagation [3-5, 15, 30]. According to the results described in this study, a Cr/Fe-depleted while Ni-enriched zone was observed ahead of all the crack tips examined (see Figs. 9 and 10). Due to the depletion of Cr in the region ahead of the crack tip, it was difficult to form a continuous and compact layer of Cr-rich oxide (discrete oxide particles) (see Fig. 6b). Since a continuous and compact layer of Cr-rich oxide is critical in protecting the material from further oxidation [13, 30, 45, 46], the grain boundary ahead of the crack tip cannot be effectively protected, resulting in the formation of an IOZ ahead of the crack tips (see Figs. 9 and 10). In addition, the localized deformation around the crack tips (see Fig. 11) was also believed to accelerate intergranular oxidation [38, 39]. After more than 50 oxidized grain boundaries were fractured by micromechanical testing in vacuum at room temperature, Dohr et al. [26] found that none of the cracks propagated beyond the intergranular oxidized portion. Based on these observations, the authors proposed that grain boundary oxidation is a prerequisite for SCC to occur and the factors that can affect oxidation can then affect crack propagation. As a result, the formation of an IOZ ahead of the crack tips might be the dominant factor that contributed to the SCC crack propagation. Since the characteristics around the SCC crack tips were similar to that reported in the literature [6, 13, 21, 24, 25], the mechanism controlling the SCC propagation of Alloy 600 in this study was proposed to be intergranular selective oxidation.

According to the recent work conducted in literature [5, 21, 22, 30, 47], the Ni-rich zone formed ahead of the crack tip was found to be the result of diffusion-induced grain boundary migration (DIGM). The authors believed that the DIGM occurred once the solute elements (such as Cr and Fe) were selectively oxidized. Since the corrosion potential used in this study was at the Ni-stable side of Ni/NiO, only Cr and Fe could be oxidized and Ni was very difficult to be oxidized, especially in the region under the surface oxide film where the corrosion potential should be even lower than in the water. As a result, it is not surprising to see DIGM in this study. In a recent work conducted by Langelier et al. [21], the authors found increased DIGM led to deeper IOZ. Thus, the authors concluded that DIGM could accelerate intergranular oxidation. However, due to the limitations of the characterization work in [21], the underlying connections between the DIGM and the accelerated intergranular oxidation was not well explained. According to the results obtained in this study, the accelerated intergranular

oxidation was found to be as a result of Cr-depletion in the DIGM zone. Once the crack propagates into the Cr-depleted zone, it is difficult for a continuous and compact Cr-rich oxide to form and then the oxidation propagates ahead of the crack tips.

### **4.3 Discrepancy in literature**

The effect of cold-worked surface on SCC have been widely studied in literature [8, 10-12, 37]. Initially, after the comparison study between a mechanical-polished surface and an electro-polished surface, the electro-polished surface was found to have higher SCC resistance because the superficial cold-worked layer was removed by electro-polishing [8, 11]. However, contrary to the literature [8, 11], Scenini et al. [10] found that a mechanical-polished surface had higher SCC resistance than an electro-polished surface, which was supported by the following researchers [12, 37]. These authors believed that the defects in the cold-worked surface could enhance the outward diffusion of Cr into the surface oxide, which would as a result lead to the formation of a more compact surface oxide and increase the SCC resistance.

This discrepancy may arise from the different extent of cold working performed in the literature [8, 10-12, 37]. The specimens with a cold-worked surface used in [8, 11] were in as-received condition (machined surface), while they were polished down to 4000 grit SiC paper in [10, 12, 37]. As a result, the extent of cold-work in the deformation layer in [8, 11] should be much greater than in [10, 12, 37]. According to the results shown in Figs. 6-8, the grain boundaries in the deformation layer had suffered severe oxidation and many SCC cracks initiated along the recrystallized grain boundaries. If recrystallization did not occur in the deformation layer, SCC resistance might be increased due to the enhanced outward diffusion of Cr along the dislocation channels in the deformation layer, as explained in [10, 12, 37]. Although TKD was not conducted in [10, 12, 37], the recrystallized grains were not expected to occur under the final polishing conditions used (4000 grit SiC paper). In conclusion, recrystallization can be expected under a machined surface [8, 11], which might decrease the SCC resistance due to the crack initiation along the recrystallized grain boundaries after severe oxidation.

### **4.4 Current understanding of the crack initiation and propagation in Alloy 600**

Based on the experimental evidence found in this study, a detailed description of SCC crack initiation and propagation in Alloy 600 with a cold-worked surface is schematically shown in Fig. 12. In our proposed model, when a coupon with a cold-worked surface (containing recrystallized grains) was exposed to PWR primary water, a thin outer surface oxide film will form on the outer surface (see Figs. 12a and b). With the increase of exposure time, intergranular oxidation will occur along the grain boundaries of the recrystallized grains in the deformation layer due to the high defect density in this area (see Fig. 12c). The intergranular oxidation in the deformation layer will continue further but is limited to the deformation layer and terminates before the deformation layer-metal matrix interface (see Fig. 12d). Since the oxide is brittle in nature, SCC cracks start to initiate along the oxidized grain boundaries under the synergistic effect of external loading and residual stress, forming microcracks on the specimen surface (see Fig. 12e). The shallow microcracks will propagate along the oxidized grain boundaries but terminate at the deformation layer-metal matrix interface (see Fig. 12f). Meanwhile, oxidation can penetrate into recrystallized grains with higher dislocation density from the intergranular oxides, resulting in intragranular oxidation. With the further increase of exposure time, although the intergranular oxidation in the deformation layer terminates at the deformation layer-matrix interface, once the intergranular oxides meet the matrix grain boundaries (Cr-depleted and high dislocation density), oxidation can further develop along them (see Fig. 12g). The external loading and residual stress will break the oxide in the matrix grain boundary and assist the further propagation of SCC cracks, leading to the formation of macrocracks (see Fig. 12h).

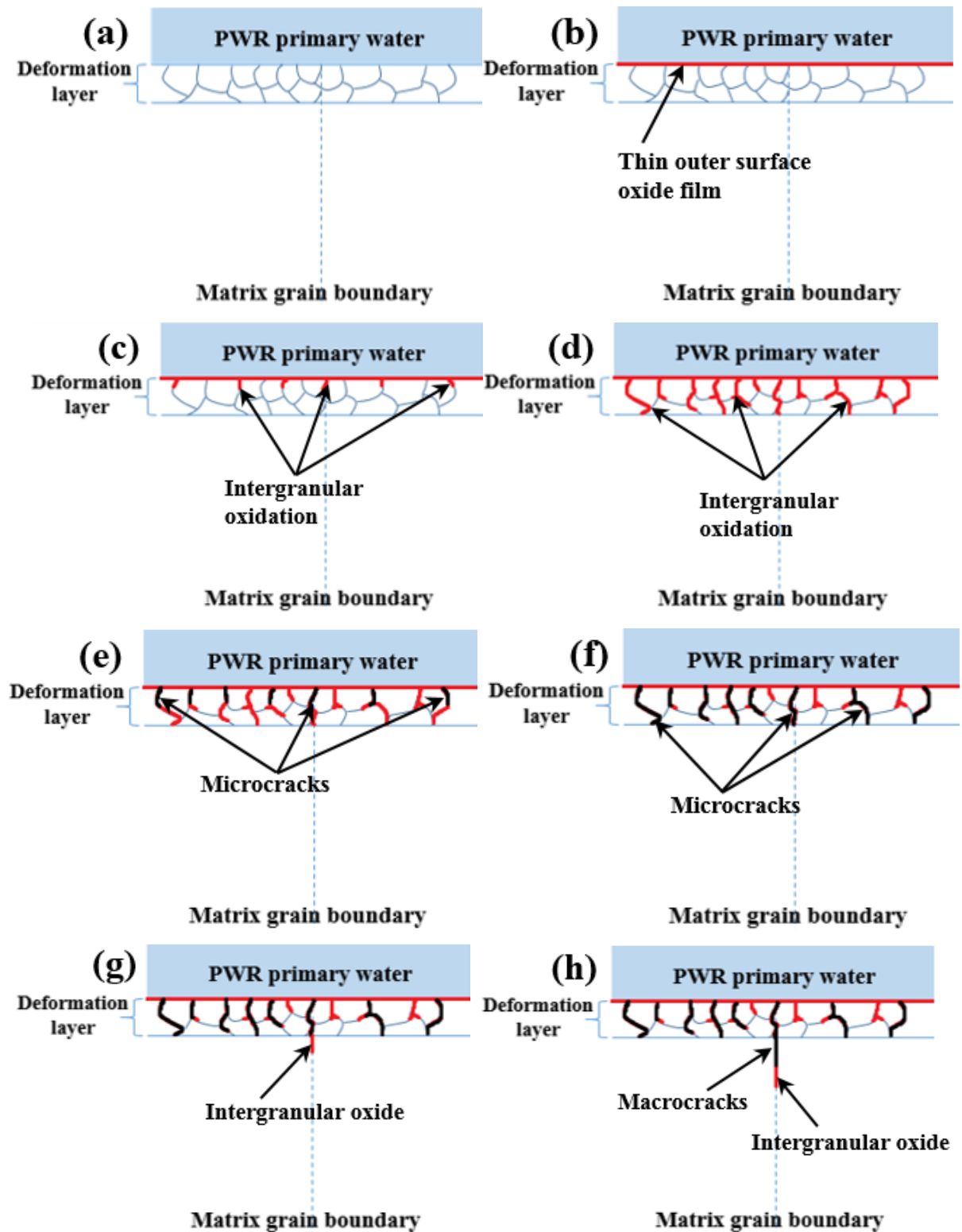


Fig. 12. Schematics showing the crack initiation (a-c) and propagation (d-f) along a matrix grain boundary from a cold-worked surface.

## 5. Conclusions

Crack initiation and propagation were observed on a cold-worked surface of Alloy 600 exposed to simulated PWR primary water at 360°C after autoclave testing. High-resolution characterization was conducted and the

following conclusions can be drawn from the investigation:

- (1) The mechanical polishing introduced a thin deformation layer on the specimen surface, where recrystallized grains were observed. The dislocation density in this zone was high, especially at the grain boundaries of the recrystallized grains.
- (2) The recrystallized grain boundaries in the deformation layer suffered selective oxidation. The intergranular oxide was porous and terminated at the deformation layer-metal matrix interface. SCC microcracks initiated along the oxidized grain boundaries under the synergistic effect of external loading and residual stress.
- (3) When the oxidation in the deformation layer met the matrix grain boundaries (with locally higher dislocation densities), the oxidation could further develop along them. Once the microcracks in the deformation layer met the oxidized matrix grain boundaries, they would propagate along these grain boundaries and form SCC macrocracks.
- (4) The oxidation in the IOZ ahead of the crack tips followed a classic internal oxidation mode, suggesting that the SCC propagation along the matrix grain boundaries could be explained by an intergranular selective oxidation mechanism.

## Acknowledgements

The authors would like to thank INSS (Japan) for providing the sample used in this study and for useful discussions. Zhao Shen is also grateful to China Scholarship Council for providing financial support. The EPSRC (EP/K040375/1, EP/N010868/1 and EP/R009392/1) grants are also acknowledged for funding this research.

## References

- [1] K. Arioka, T. Yamada, T. Miyamoto, M. Aoki. Intergranular Stress Corrosion Cracking Growth Behavior of Ni-Cr-Fe Alloys in Pressurized Water Reactor Primary Water. *Corrosion*, 70(2014): 695-707.
- [2] S.M. Bruemmer, L.E. Thomas. High-resolution analytical electron microscopy characterization of corrosion and cracking at buried interfaces. *Surface and interface analysis*, 31(2001): 571-581.
- [3] Z. Shen, K. Arioka, S. Lozano-Perez. A mechanistic study of SCC in Alloy 600 through high-resolution characterization. *Corrosion Science*, 132(2018): 244-259.
- [4] Y.S. Lim, H.P. Kim, S.S. Hwang. Microstructural characterization on intergranular stress corrosion cracking of Alloy 600 in PWR primary water environment. *Journal of Nuclear Materials*, 440(2013): 46-54.
- [5] S.M. Bruemmer, M.J. Olszta, M.B. Toloczko, D.K. Schreiber. Grain Boundary Selective Oxidation and Intergranular Stress Corrosion Crack Growth of High-Purity Nickel Binary Alloys in High-Temperature Hydrogenated Water. *Corrosion Science*, 131(2018): 310-323.
- [6] G. Bertali, F. Scenini, M. G. Burke. Advanced microstructural characterization of the intergranular oxidation of Alloy 600. *Corrosion Science*, 100 (2015): 474-483.
- [7] P.L. Andresen, M.M. Morra. Stress corrosion cracking of stainless steels and nickel alloys in high-temperature water. *Corrosion*, 64 (2008): 15-29.
- [8] S.L. Hong. Influence of surface condition on primary water stress corrosion cracking initiation of alloy 600. *Corrosion*, 57(2001): 323-333.
- [9] Y.L. Han, J.N. Mei, Q.J. Peng, E.H. Han, W. Ke. Effect of electropolishing on corrosion of Alloy 600 in high temperature water. *Corrosion Science*, 98 (2015): 72-80.
- [10] F. Scenini, R.C. Newman, R.A. Cottis, R.J. Jacko. Effect of surface preparation on intergranular stress corrosion cracking of alloy 600 in hydrogenated steam. *Corrosion*, 64(2008): 824-835.
- [11] P.M. Scott, C. Benhamou. An overview of recent observations and interpretations of IGSCC in nickel base



alloys in PWR primary water. In Proc. of the 10th International Symposium on Environmental Degradation of Materials in Nuclear Power Systems-Water Reactors, TMS, 2001.

[12] Z. Zhai, M.B. Toloczko, M.J. Olszta, S.M. Bruemmer. Stress corrosion crack initiation of alloy 600 in PWR primary water. *Corrosion Science*, 2017(123): 76-87.

[13] G. Bertali, F. Scenini, M.G. Burke. The effect of residual stress on the Preferential Intergranular Oxidation of Alloy 600. *Corrosion Science*, 111(2016): 494-507.

[14] K. Arioka, T. Yamada, T. Terachi, T. Miyamoto. Dependence of stress corrosion cracking for cold-worked stainless steel on temperature and potential, and role of diffusion of vacancies at crack tips. *Corrosion*, 64(2008): 691-706.

[15] M. Meisnar, A. Vilalta-Clemente, M. Moody, K. Arioka, S. Lozano-Perez. A mechanistic study of the temperature dependence of the stress corrosion crack growth rate in SUS316 stainless steels exposed to PWR primary water. *Acta Materialia*, 114 (2016): 15-24.

[16] P.M. Scott, M. Le Calver. "Some possible mechanisms of intergranular stress corrosion cracking of alloy 600 in PWR primary water". In Proceedings of the sixth international symposium on environmental degradation of materials in nuclear power systems-water reactors, (TMS, 1993), 657-665.

[17] H.K. Birnbaum, P. Sofronis. Hydrogen-enhanced localized plasticity—a mechanism for hydrogen-related fracture. *Materials Science and Engineering: A*, 176(1994): 191-202.

[18] F.P. Ford. Quantitative prediction of environmentally assisted cracking. *Corrosion*, 52(1996): 375-395.

[19] H. Xue, Z. Li, X. Xue, Z. Lu, T. Shoji. Further understanding on deformation-oxidation model in stress corrosion cracking tip based on meso-scale mechanical field. In ASME 2011 Pressure Vessels and Piping Conference, pp. 631-637. American Society of Mechanical Engineers, 2011.

[20] K. Arioka, T. Miyamoto, T. Yamada, M. Aoki. Role of cavity formation in crack initiation of cold-worked carbon steel in high-temperature water. *Corrosion*, 69(2013): 487-496.

[21] B. Langelier, S.Y. Persaud, A. Korinek, T. Casagrande, R.C. Newman, G. A. Botton. Effects of boundary migration and pinning particles on intergranular oxidation revealed by 2D and 3D analytical electron microscopy. *Acta Materialia*, 131(2017): 280-295.

[22] M.G. Burke, G. Bertali, E. Prestat, F. Scenini, S.J. Haigh. The application of in situ analytical transmission electron microscopy to the study of preferential intergranular oxidation in Alloy 600. *Ultramicroscopy*, 176(2017): 46-51.

[23] P.M. Scott. An overview of internal oxidation as a possible explanation of intergranular stress corrosion cracking of alloy 600 in PWRs. In Ninth International Symposium on Environmental Degradation of Materials in Nuclear Power Systems—Water Reactors (pp. 1-14). Hoboken, NJ, USA: John Wiley & Sons, Inc., 1999.

[24] S.Y. Persaud, A. Korinek, J. Huang, G.A. Botton, R.C. Newman. Internal oxidation of Alloy 600 exposed to hydrogenated steam and the beneficial effects of thermal treatment. *Corrosion Science*, 86(2014): 108-122.

[25] M. B. Capell, G.S. Was. Selective internal oxidation as a mechanism for intergranular stress corrosion cracking of Ni-Cr-Fe alloys, *Metall. Mater. Trans. A*, 38(2007): 1244-1259.

[26] J. Dohr, D.E. Armstrong, E. Tarleton, T. Couvant, S. Lozano-Perez. The influence of surface oxides on the mechanical response of oxidized grain boundaries. *Thin Solid Films*, 632(2017): 17-22.

[27] K. Fujii, T. Miura, H. Nishioka, K. Fukuya. Degradation of grain boundary strength by oxidation in alloy 600. *Materials transactions*, 52(2011): 1447-1458.

[28] H. Dugdale, D.E. Armstrong, E. Tarleton, S.G. Roberts, S. Lozano-Perez. How oxidized grain boundaries fail. *Acta Materialia*, 61(2013): 4707-4713.

- [29] C. Wagner. Reaktionstypen bei der Oxydation von Legierungen. *Zeitschrift für Elektrochemie, Berichte der Bunsengesellschaft für physikalische Chemie*, 63(1959): 772-782.
- [30] W. Kuang, M. Song, G.S. Was. Insights into the stress corrosion cracking of solution annealed alloy 690 in simulated pressurized water reactor primary water under dynamic straining, *Acta Materialia*, 151(2018): 321-333.
- [31] L. Marchetti, S. Perrin, F. Jambon, M. Pijolat. Corrosion of nickel-base alloys in primary medium of pressurized water reactors: New insights on the oxide growth mechanisms and kinetic modelling. *Corrosion Science*, 102(2016): 24-35.
- [32] H. Lefaix-Jeuland, L. Marchetti, S. Perrin, M. Pijolat, M. Sennour, R. Molins. Oxidation kinetics and mechanisms of Ni-base alloys in pressurised water reactor primary conditions: Influence of subsurface defects. *Corrosion Science*, 53(2011): 3914-3922.
- [33] S. Ghosh, M.K. Kumar, V. Kain. High temperature oxidation behavior of AISI 304L stainless steel—Effect of surface working operations. *Applied Surface Science*, 264(2013): 312-319.
- [34] S. Wang, Y. Hu, K. Fang, W. Zhang, X. Wang. Effect of surface machining on the corrosion behaviour of 316 austenitic stainless steel in simulated PWR water. *Corrosion Science*, 126(2017): 104-120.
- [35] G. Han, Z. Lu, X. Ru, J. Chen, Q. Xiao, Y. Tian. Improving the oxidation resistance of 316L stainless steel in simulated pressurized water reactor primary water by electropolishing treatment. *Journal of Nuclear Materials*, 467(2015): 194-204.
- [36] S. Cissé, L. Laffont, B. Tanguy, M.C. Lafont, E. Andrieu. Effect of surface preparation on the corrosion of austenitic stainless steel 304L in high temperature steam and simulated PWR primary water. *Corrosion Science*, 56(2012): 209-216.
- [37] R. Morris, N. Lewis, D.S. Morton. 3D analysis of surface treatment effects on the oxidation of grain boundaries in Alloy 600. In: *Proceedings of the 16th International Symposium on Environmental Degradation of Materials in Nuclear Power Systems-Water Reactors*, Ashville, NC, USA, TMS/NACE, 2013.
- [38] S. Lozano-Perez, K. Kruska, I. Iyengar, T. Terachi, T. Yamada. The role of cold work and applied stress on surface oxidation of 304 stainless steel. *Corrosion Science*, 56(2012): 78-85.
- [39] T. Terachi, T. Yamada, T. Miyamoto, K. Arioka. SCC growth behaviors of austenitic stainless steels in simulated PWR primary water. *Journal of Nuclear Materials*, 426(2012): 59-70.
- [40] R.C. Newman, T.S. Gendron, P.M. Scott. Internal oxidation and embrittlement of Alloy 600, in *9th International Symposium on Environmental Degradation of Materials in Nuclear Power Systems-Water Reactors*, Newport Beach, CA, USA, 1999.
- [41] B. Langelier, S.Y. Persaud, R.C. Newman, G.A. Botton. An atom probe tomography study of internal oxidation processes in Alloy 600. *Acta Materialia*, 109(2016): 55-68.
- [42] M. Sennour, P. Laghoutaris, C. Guerre, R. Molins. Advanced TEM characterization of stress corrosion cracking of Alloy 600 in pressurized water reactor primary water environment. *Journal of Nuclear Materials*, 393(2009): 254-266.
- [43] A. Stratulat, J.A. Duff, T.J. Marrow. Grain boundary structure and intergranular stress corrosion crack initiation in high temperature water of a thermally sensitised austenitic stainless steel, observed in situ. *Corrosion Science*, 8(2014): 428-435.
- [44] D.C. Crawford, G.S. Was. The role of grain boundary misorientation in intergranular cracking of Ni-16Cr-9Fe in 360°C Argon and high-purity water. *Metallurgical Transactions A*, 23(1992): 1195-1206.
- [45] S.M. Bruemmer, B.W. Arey, L.A. Charlot. Influence of chromium depletion on intergranular stress corrosion cracking of 304 stainless steel. *Corrosion*, 48(1992): 42-49.

- [46] Z. Shen, M. Meisnar, K. Arioka, S. Lozano-Perez. Mechanistic understanding of the temperature dependence of crack growth rate in alloy 600 and 316 stainless steel through high-resolution characterization. *Acta Materialia*, 165(2019): 73-86.
- [47] Z. Shen, P. Karamched, K. Arioka, S. Lozano-Perez. Observation and quantification of the diffusion-induced grain boundary migration ahead of SCC crack tips. *Corrosion Science*. 147(2019): 163-168.

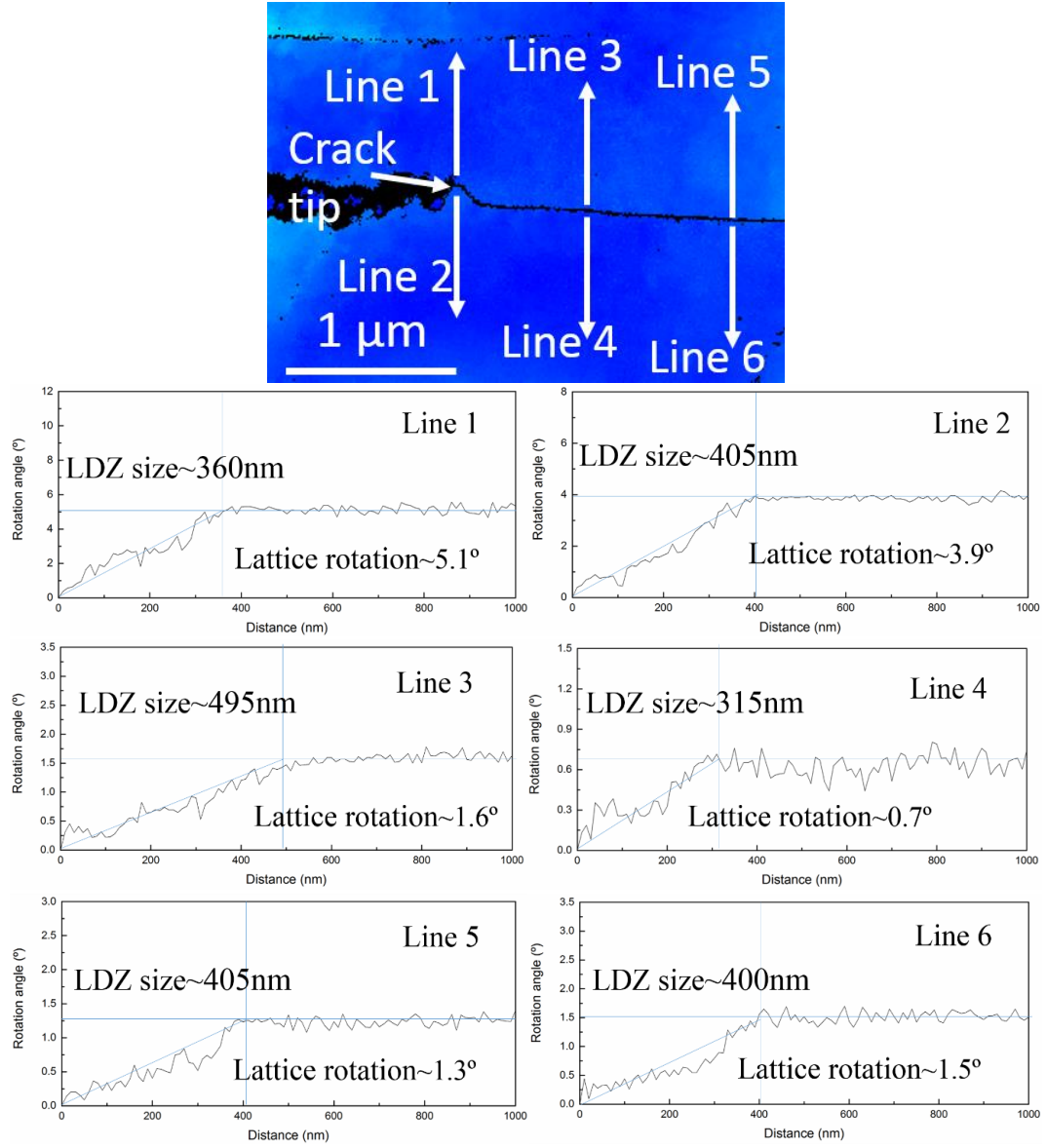


Fig. S1. The comparison of the extent of localized deformation around a crack tip and at the grain boundary ahead of the crack tip: (a) MO map; (b) MO line profiles.